HHS Public Access

Author manuscript

*Biochemistry*. Author manuscript; available in PMC 2016 December 07.

Published in final edited form as:

*Biochemistry*. 2016 March 01; 55(8): 1265–1278. doi:10.1021/acs.biochem.5b01255.

# All the $O_2$ consumed by Thermus thermophilus cytochrome $ba_3$ is delivered to the active site through a long, open hydrophobic tunnel with entrances within the lipid bilayer

**Paween Mahinthichaichan**, **Robert B. Gennis***, and **Emad Tajkhorshid***

Department of Biochemistry, and Beckman Institute for Advanced Science and Technology, University of Illinois at Urbana-Champaign, Urbana, IL 61801, U.S.A

## Abstract

Cytochrome $ba_3$ is a proton-pumping heme-copper oxygen reductase from the extreme thermophile *Thermus thermophilus*. Despite the fact that the enzyme's active site is buried deep within the protein, the apparent second order rate constant for the initial binding of $O_2$ to the active-site heme has been experimentally found to be $10^9$ $M^{-1}s^{-1}$ at 298 K, at or near the diffusion limit, and two orders of magnitude faster than for $O_2$ binding to myoglobin. To provide quantitative and microscopic descriptions of the $O_2$ delivery pathway and mechanism in cytochrome $ba_3$, extensive molecular dynamics simulations of the enzyme in its membrane-embedded form have been performed, including different protocols of explicit ligand sampling (flooding) simulations with $O_2$, implicit ligand sampling analysis and *in silico* mutagenesis. The results show that $O_2$ diffuses to the active site exclusively via a Y-shaped hydrophobic tunnel with two 25-Å long membrane-accessible branches that coincide with the pathway previously suggested by the crystallographically identified xenon binding sites. The two entrances of the bifurcated tunnel of cytochrome $ba_3$ are located within the lipid bilayer, where $O_2$ is preferentially partitioned from the aqueous phase. The largest barrier to $O_2$ migration within the tunnel is estimated to be only 1.5 kcal/mol, allowing $O_2$ to reach the enzyme active site virtually impeded by one-dimensional diffusion once it reaches a tunnel entrance at the protein surface. Unlike other $O_2$-utilizing proteins, the tunnel is "open" with no transient barriers observed due to protein dynamics. This unique low-barrier passage through the protein assures that $O_2$ transit through the protein is never rate-limiting.

## Graphical Abstract

r-gennis@illinois.edu; emad@life.illinois.edu, Phone: +1 217 3339075; +1 217 2446914.

**Supporting Information Available**

Supp. Fig. 1–7 This material is available free of charge via the Internet at http://pubs.acs.org/.

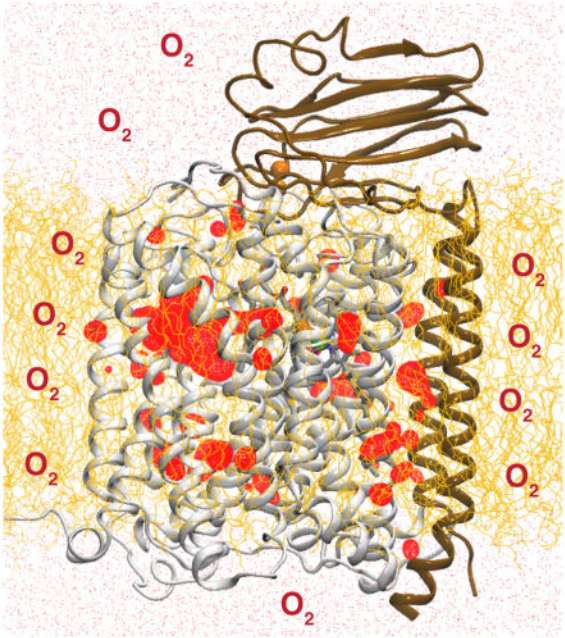


## Introduction

The heme-copper oxygen reductases (HCOs) are integral membrane enzyme complexes that catalyze the exergonic reduction of $O_2$ to water and terminate the aerobic respiratory chains of all aerobic eukaryotes and most aerobic prokaryotic organisms.[1–9] These enzymes include the mitochondrial as well as all bacterial cytochrome c oxidases. The free energy release from the reduction of $O_2$ is used to generate a proton motive force across biological membranes which, in turn, drives ATP biosynthesis, as well as other energy-requiring processes.[2,10–13] The HCOs, together with closely related NO reductases (NORs), are members of the heme-copper superfamily[5,10–13] which have in common a membrane subunit (Subunit I) with a minimum of 12 transmembrane $\alpha$-helical spans, which contains the bimetallic active site where $O_2$ (or NO) binds and is reduced to water (or $N_2O$). For the $O_2$ reductases (HCOs), the bimetallic active site consists of a heme Fe (e.g. heme $a_3$) and a nearby Cu atom (4–5Å distant). $O_2$ binds to an open axial coordination site on the reduced heme Fe and is reduced by a sequence of proton-coupled electron transfer reactions. The heme-copper active site is deeply buried within the membrane subunit but must allow rapid access for each of the substrates of the reaction.

$$4e^{-}(cytc)+4H^{+}+O_2 \rightarrow 2H_2O$$

The active site of many enzymes are sequestered from the bulk solution, necessitating efficient strategies by which the substrates can be delivered and products removed. These strategies include hydrophilic clefts or pores or hydrophobic tunnels or cavities which allow the substrate to diffuse towards (or products away from) the active site.[14–18] Most often the pathways are gated by protein conformational changes that may be large, as in movement of

a protein domain sealing the active sites, or may be small, as in single amino acid side chain fluctuations allowing passage of a small molecule between cavities within the protein, en route to the active site.[18–20]

The three substrates that must access the active site of the HCOs are $O_2$, protons and electrons. Electrons are delivered to the active site one at a time by a linear sequence of proton-coupled, step-wise electron transfer reactions between redox-active metal centers from the site where cytochrome c is oxidized (on Subunit II).[21] Protons are delivered to the active site through one or two different proton-conducting channels (depending on the enzyme) that have entrances at the aqueous phase on the electrically negative side of the membrane (e.g., bacterial cytoplasm or mitochondrial matrix). Conserved polar residues as well as internal water molecules provide the continuous hydrogen-bond networks needed for the long-range (25–30Å) proton diffusion to the active site by the Grotthus mechanism.[6,7,22–25] In contrast to the electron and protons "wires", pathways for $O_2$ diffusion into the active site have not been well-characterized. Hydrophobic tunnels in the X-ray structures of the aerobic respiratory heme-copper oxygen reductases,[26–32] including cytochrome $ba_3$ from *Thermus thermophilus*,[28,31,33,34] have been suggested as putative $O_2$ tunnels. Xenon (Xe), which has a similar size as $O_2$, is often used in crystallographic studies to locate hydrophobic cavities that may provide binding sites for small diatomic gas molecules, including $O_2$, CO, $H_2$ or $N_2$.[35–39] X-ray crystallography has located Xe binding sites in both cytochrome $ba_3$ [35,40] and the $aa_3$-type oxygen reductase from *Rhodobacter sphaeroides*,[29] thereby identifying hydrophobic cavities that are within their putative $O_2$ tunnels.

Recent molecular dynamics (MD) simulations and computational analyses of the HCO from *Rhodobacter sphaeroides* concluded that the putative $O_2$ tunnel suggested by X-ray crystallography is not the primary pathway by which $O_2$ reaches the active site.[41] Two additional pathways, which are not apparent in the static X-ray structures and may be formed transiently by protein dynamics, were suggested as more likely pathways that lead $O_2$ to the enzyme's active site. Hence, what appears to be an $O_2$ pathway may not function as such.

In the present study, we computationally examine $O_2$ pathways to the active site of a different respiratory HCO, cytochrome $ba_3$ from the hyperthermophile *Thermus thermophilus*. Similar to HCO from *R. sphaeroides*, Xe binding sites have been identified by X-ray crystallography that align within a hydrophobic tunnel suggested to act as the $O_2$ pathway.[35,40] In addition apparent second order rate constant for $O_2$ binding to the active site from solution has been directly measured to be $1\times10^9$ $M^{-1}s^{-1}$ at 298 K,[42,43] near the diffusion limit and far greater than found for $O_2$ diffusion to internal sites within other proteins, including myoglobin ($1.6\times10^7$ $M^{-1}s^{-1}$).[44] The motivation of this study is to understand how $O_2$ reaches the deeply buried active site of cytochrome $ba_3$ so rapidly.

Previous studies have characterized mutants that place bulky residues within the putative $O_2$ tunnel that reduce the apparent rate constant 5-fold,[33] supporting the X-ray observed tunnel as a functional $O_2$ pathway in cytochrome $ba_3$. Short (1 ns) MD simulations concentrating on the dynamics and stability of $O_2$ at Xe binding sites of the X-ray tunnel indicated that $O_2$

can rapidly move between individual Xe sites within the hydrophobic tunnel.[33] In the present study, extensive MD simulations (repeated 50-ns simulations with multiple copies of $O_2$) as well as implicit ligand sampling (ILS)[45] are used to characterize the energetics of $O_2$ partitioning within the protein and the trajectories of $O_2$ molecules starting outside the protein and reaching the active site. The all-atom MD was performed using the entire 3-subunit protein embedded in a lipid bilayer and surrounded by a bulk aqueous solution. The study demonstrates that the substrate $O_2$ utilizes the X-ray Xe-bound hydrophobic tunnel as the pathway for reaching the active site. Furthermore, unlike other proteins, such as myoglobin or the *R. sphaeroides* HCO, the $O_2$ pathway in cytochrome $ba_3$ is static and does not seem to be affected by protein dynamics. The highest free energy barrier for $O_2$ to diffuse through the identified $O_2$ pathway is calculated to be 1.5 kcal/mol. Cytochrome $ba_3$, therefore, appears to have evolved so that the transit time of $O_2$ through the 25-Å long hydrophobic tunnel is never rate-limiting. Under 298 K, the enzyme is limited by the rate of chemical catalysis ($k_{cat} \approx 10^2\ s^{-1}$) at $O_2$ concentration above 0.1 $\mu$M, and would be limited by the rate of $O_2$ reaching the entrances of the $O_2$ pathway when $O_2$ concentration is below 0.1 $\mu$M. At physiological conditions (343–363 K) where the organism (*T. thermophilus*) grows, the enzyme velocity may be limited by the rate of $O_2$ reaching the pathway's entrances.

## Materials and Methods

### Construction of the membrane-embedded cytochrome $ba_3$ model

MD simulations were performed on a membrane-embedded model of the cofactor-bound cytochrome $ba_3$ complex constructed using the crystal structure of the enzyme from *T. thermophilus* HB8 strain (PDB entry 1XME)[46] inserted into a hydrated and ionized patch of POPE (1-palmitoyl-2-oleoyl-sn-glycero-3-phosphoethanolamine) bilayer. The crystal structure contains three subunits (I, II and IIa), 75 water molecules, heme b, active-site heme $a_3$, three copper ions ($Cu_B$ and dicopper $Cu_A$) cofactors. The membrane-embedded cytochrome $ba_3$ was constructed using VMD.[47]

The cofactor-bound cytochrome $ba_3$ complex was embedded in a patch of POPE membrane by aligning the center of transmembrane regions of its subunits I, II and IIa with the midpoint of the membrane. Lipids that overlapped the protein were removed, keeping 98 lipids in the periplasmic leaflet and 92 lipids in the cytoplasmic leaflet. The membrane-embedded cytochrome $ba_3$ was then solvated with water. Water molecules that were in the membrane were removed, keeping 15,177 water molecules. Finally, 0.2M NaCl (26 $Na^+$ and 33 $Cl^-$ ions) was added to neutralize and ionize the complex, resulting in a fully solvated model of approximately 85,000 atoms.

### Simulation protocols

MD simulations consisted of the following steps: (1) 0.5-ns melting of lipid tails during which only the lipid tails were allowed to move in order to achieve better packing of lipids around the inserted protein; (2) 0.5-ns simulation with restraints ($k$ =1 kcal/mol/Å$^2$) applied to heavy atoms of the protein and cofactors (all lipid atoms and water moving) and with harmonic potentials ($k$ =0.1 kcal/mol/Å$^2$) applied to keep water out of the membrane; (3)

0.5-ns simulations with only backbone atoms of the protein and heavy atoms of the cofactors restrained ($k$ =1 kcal/mol/Å$^2$); (4) 1-ns simulation with only $C_\alpha$ atoms of the protein and heavy atoms of the cofactors restrained; and (5) 20-ns unrestrained relaxation. Energy minimization (1,000 steps) was performed at the beginning of Steps 1, 2 and 3 using the conjugate gradient algorithm. In order to maintain the ligation of $Cu_B$ to H233, H282 and H283, the His-$Cu_B$ connections were described as bonds with $k$ =65 kcal/mol/Å$^2$ for the bonds and $k$ =30 kcal/mol/rad$^2$ for the angles involving the His-$Cu_B$ bond.

All simulations were performed using NAMD2[48] with a time step of 2 fs. The periodic boundary conditions (PBC) were used throughout the simulations. All bonds involving hydrogen atoms were kept rigid using the SHAKE algorithm.[49] To evaluate long-range electrostatic interactions in PBC without truncation, the particle mesh Ewald (PME) method[50] with a grid density of 1/Å$^3$ was used. The cutoff for van der Waals interactions was set at 12Å. All of simulation steps except the melting of lipid tails (Step 1) were performed in a flexible cell, which allows the membrane-embedded cytochrome $ba_3$ model to change its dimensions independently, and were performed under NPT ensemble. The temperature was maintained at 310K by Langevin dynamics[51] with a damping coefficient $\gamma$ of 1/ps. The Nosé-Hoover Langevin piston method[51,52] with a piston period of 200 fs was used to maintain the pressure at 1 atm.

The CHARMM22 force field with $\phi/\psi$ corrections[53,54] was used to describe the protein and heme cofactors, and CHARMM36[55] was used to describe the lipids. The TIP3P model[56] was used as the water model. All cofactors were treated in the reduced state. The force field parameters for the hydroxyethylfarnesyl side chain of the active-site heme cofactor (heme $a_3$), which were not available in the CHARMM force field library, were constructed by analogy using parameterized alcohol, alkene, and alkane fragments.[57] The parameters for the copper ions were those previously used by Hofacker and Schulten.[58] A harmonic potential (k=400 kcal/mol/Å$^2$) was used for the $N_\varepsilon$-$C_\varepsilon$ bond of the His-Tyr (H233–Y237) crosslink.[59]

Analyses were performed mainly with VMD[47] and MATLAB. The pore profile for $O_2$ pathway was calculated using the MolAxis program,[60] which was previously used to probe for tunnels in several proteins.[61,62]

## Production runs

The final frame of wild-type cytochrome $ba_3$ from the 20-ns relaxation simulation was used as the starting configuration for the explicit ligand sampling simulations (ELS, aka flooding simulations[63,64] ) in which $O_2$ molecules were added, for the continued 50-ns simulation in the absence of $O_2$ (apo), and for *in silico* mutagenesis.

### Explicit ligand sampling (ELS) simulations

**Long simulations:** To probe for $O_2$ delivery pathways of cytochrome $ba_3$ and characterize $O_2$ delivery process, 100 $O_2$ molecules, corresponding to 0.21M [$O_2$] calculated with respect to the total simulation box volume of 790,000Å$^3$, were added to the equilibrated membrane-embedded enzyme model. This $O_2$ concentration is 161-fold higher than the saturated $O_2$

concentration in water at ambient conditions. This high $O_2$ concentration was introduced to maximize the sampling of $O_2$ delivery pathways in the protein within limited timescale (tens of nanoseconds). Three independent simulation systems were designed in which $O_2$ molecules were initially distributed in the membrane and aqueous phases at different ratios: 70:30, 100:0 and 0:100. Each system was visually inspected to ensure that the added $O_2$ molecules do not overlap with atoms of other molecules, and was then simulated for 50 ns (Fig. 1a). As all three simulation systems showed that approximately 80 of 100 $O_2$ molecules localized in the membrane after reaching a steady distribution (Fig. 1b), the 70:30 ratio system was repeated two more times, resulting in a total of 5×50 ns simulations. Repeated simulations are to improve statistics and provide more accurate descriptions of thermodynamic properties associated the $O_2$ delivery. To identify $O_2$ delivery pathways, a 3D density map representing the $O_2$ occupancy profiles was calculated using the Volmap tool in VMD. Using equilibrated fractions (last 40 ns) of the MD trajectories, the map was projected as a free-energy ($\Delta G_{i,sol}$) map, which describes the energetics of $O_2$ insertion.

$$\Delta G_{i,sol} = -RT \ln \frac{p_i}{p_{sol}}$$

$p_i$ represents the probability of finding $O_2$ at a site $i$ calculated over the equilibrated trajectories. $p_{sol}$ is probability of finding $O_2$ in the bulk aqueous solution. $p_{sol}$ = 0.00035, determined from the simulation, was used as the reference for estimating partitioning free energies of $O_2$, as $O_2$ appears to distribute uniformly in the aqueous phase whereas it is heterogeneously distributed in the membrane, potentially due to various degrees of hydrophobicity in different regions of the membrane (Fig. 1a). For simulations including the protein, $O_2$ was considered to reach the active site of the enzyme when either one of its oxygen atoms was within 6Å of $Cu_B$. Their entries were confirmed by visually monitoring all delivered $O_2$ molecules through MD trajectories and their separation from $Cu_B$. For the re-entry of $O_2$, if $O_2$ first moves away from $Cu_B$ by more than 30Å which is already outside the protein and later diffuses into the active site, we considered it as an independent (re-entry) event.

**Short simulations:** Once the $O_2$ delivery pathway was identified, the time of $O_2$ diffusing from outside of the protein to the active site, which can relate MD simulation results to time-resolved spectroscopic experiments, can be estimated.[42,43] To improve statistics, a set of 21 independent short (each 3–5 ns) simulations was performed. To reduce the computational costs, these new simulations were terminated once one $O_2$ reached the active site, which was determined by its presence within 6Å of $Cu_B$. They were all initiated with 90 $O_2$ in the membrane and 10 in the aqueous phase corresponding to the upper equilibrium ratio of 90:10 obtained from the 50-ns long simulations. A 0.5-ns pre-equilibration was then performed for each system to allow further randomizing of $O_2$ molecules. A different random number seed was assigned to initialize each production run. From these short simulations, the time to observe the first $O_2$ to reach the active site after the start of a simulation is referred to as “first entry time” or $t_{first}$. The transit time of $O_2$ diffusion to the

entrance of the pathway ($t_{out \rightarrow ent}$) and the transit time of $O_2$ diffusion from the entrance to the active site ($t_{ent \rightarrow cat}$) can also be estimated.

**Implicit ligand sampling (ILS) calculations:** The implicit ligand sampling (ILS) method[45] was employed as an alternative, complementary method to the ELS simulations to characterize $O_2$ delivery pathways of cytochrome $ba_3$. ILS is a quantitative method for characterizing gas migration pathways[65–68] that might be difficult to probe with conventional MD simulations (i.e., ELS) due to limited sampling. The method is only applicable to ligands that have weak interactions with proteins. As previously described,[45] ILS calculates ligand-interaction energies ($E_i$) at all sites of each subgrid averaged over an ensemble of protein conformations and ligand orientations, which estimate the probability of finding a ligand in a particular subgrid ($p_i$) and then the free energy of inserting ligand into that subgrid ($\Delta G_i$).

$$\Delta G_i = -RT \ln \frac{p_i}{p_0} = -RT \ln \frac{<e^{-E_i/RT}>}{p_0}$$

where $p_0$ (in vacuum)=1.

The apo trajectory of cytochrome $ba_3$, which was simulated in the absence of $O_2$ for 50 ns following the 20-ns relaxation simulation, was used for ILS calculations to characterize potential $O_2$ delivery pathway. A $60 \times 65 \times 85 Å^3$ grid was placed on the cytochrome $ba_3$ complex covering portions of the membrane and aqueous phases. The grid, which defines where $O_2$ molecules were sampled and consists of several subgrids, was $331{,}500 Å^3$. Each subgrid contained $3 \times 3 \times 3$ interaction sites. Ten orientations of $O_2$ were sampled in all 27 interaction sites of a subgrid over 5,000 frames. The solvation free energy of $O_2$ ($\Delta G_{sol}$) was used as the reference for calculating the partitioning free energy of $O_2$ ($\Delta G_{i,sol}$).

$$\Delta G_{i,sol} = \Delta G_i - \Delta G_{sol}$$

We calculated $\Delta G_{sol}$ using free-energy perturbation (FEP)[69] and ILS methods over a $30 \times 30 \times 30 Å^3$ ionized water box. Both methods yielded $\Delta G_{sol}$ of 2.1 kcal/mol.

***In silico* site-directed mutagenesis:** To examine the role of the identified $O_2$ pathway of cytochrome $ba_3$ in facilitating the delivery of the substrate $O_2$, aliphatic residues along the pathway (I78, V79, A120, A149, S150 and L200) were individually mutated to either a phenylalanine or a tryptophan. These residues were characterized as lining residues by the ELS simulations and ILS calculations of the wildtype enzyme. Four single (I78F, A120F, A149F, S150W), two double (A120F/S150W and V79F/S150W) and one triple (I78F/V79F/L200F) mutants were modeled and simulated. Each mutant was energy-minimized for 1,000 steps, and equilibrated for at least 10 ns. ILS was employed to assess the effects of the mutations by exploring the free energy of $O_2$ partitioning in the pathway. In addition, ELS simulations were performed to locate $O_2$ delivery pathways and estimate transit times of $O_2$ diffusion into the active site.

**Simulations of $O_2$ in protein-free membrane:** We also performed simulations of a protein-free membrane system in order to calculate the partitioning profiles of $O_2$ between the membrane and aqueous phases (without any perturbation caused by the protein in the lipid structure) and to compare the results with those previously obtained from experiments and MD simulations.[70–74] The protein-free membrane model was composed of 40,666 atoms (172 POPE lipids, 6,372 water molecules, 24 $Na^+$, and 24 $Cl^-$ ions). The 0.5-ns melting of lipid tails, 5-ns relaxation and 10-ns production simulations were performed as described above. The 10-ns production trajectory was analyzed by ILS for $O_2$ insertion. Then, two independent ELS simulations were performed starting from the 5-ns apo relaxation step: one with 100 $O_2$ initially in the aqueous phase, and one with 100 $O_2$ initially in the membrane. The $O_2$ concentration calculated with respect to the total volume of 435,000$Å_3$ was 0.38 M. A 0.1-ns equilibration at 400K followed by a gradual cooling from 400K to 310K with the total time of 0.2 ns was performed to allow rapid randomizing of $O_2$. 50-ns production simulations were performed after the cooling. The partition coefficient of $O_2$ was determined from the ratio of $O_2$ in the membrane to the aqueous phase. $O_2$ was considered to be in the membrane when either oxygen atom in the molecule resided between the C22 atoms ($C_\alpha$ of the palmitate's ester) of the POPE lipids in both leaflets or $-16Å \leq z \leq 16Å$ (Fig. 1a). With the estimated volume of the aqueous phase of 210,000$Å^3$ being slightly smaller than that of the membrane, the number of $O_2$ residing in the aqueous phase must be multiplied by a factor of 1.1 to calculate the partition coefficient.

## Results

### Partitioning of $O_2$ between the membrane and aqueous phases

Before starting the ELS simulations on cytochrome $ba_3$, we determined the partition coefficient of $O_2$ between the membrane and aqueous phases using the protein-free membrane system (Fig. 1a). The total volume of this system, 435,000$Å^3$, consists of water and phospholipids in a volume ratio of approximately 9:10. 100$O_2$ molecules or 380mM [$O_2$] were added and allowed to distribute in the system for 50 ns. Starting with different initial distributions of the $O_2$ molecules in the membrane and aqueous phases (100:0 or 0:100) yielded the same equilibrium distribution within 10 ns, with approximately 85 $O_2$ molecules in the membrane and 15 in the aqueous phase (Supp. Fig. 1). After normalizing to the volumes of the aqueous and membrane phases, the ratio of concentrations gives a partition coefficient of 5.5 for $O_2$ favoring the membrane, close to the values obtained previously in a similar simulation study performed in the absence of a protein, 4.7,[65] and still comparable to the experimental value of 3.9 estimated using fluorescence quenching.[71] The equilibrium profile of $O_2$ distribution within the membrane was also calculated independently using the ELS trajectories and ILS (Fig. 1a). The results are equivalent to those reported previously for simulations with just the aqueous solution and phospholipid[65] and also agree with experimental data using NMR and ESR.[73,74]

For the membrane-embedded complex of cytochrome $ba_3$, the total volume of the simulation system, 790,000$Å^3$ yields an $O_2$ concentration of 210mM (100 $O_2$ molecules) incorporated in the system. Similar to the system, different initial distributions of the $O_2$ molecules in the protein-free membrane and aqueous phases resulted in the same equilibrium distribution

with approximately 80 $O_2$ molecules in the membrane-protein phase and 20 in the aqueous phase (Fig. 1b). Since the volume ratio of the aqueous phase to the combined membrane-protein phase is 9:7, the equilibrium concentration of $O_2$ in the aqueous phase has to be normalized, yielding a partition coefficient of 5.2 which is in comparable to that of the protein-free system and previous studies.[65,71]

## $O_2$ pathway to the active site

$O_2$ access to the active site of cytochrome $ba_3$ was monitored in ELS trajectories starting with 100 $O_2$ molecules distributed between the membrane and aqueous phases, but not within the protein. Regardless of the initial $O_2$ distribution, the first $O_2$ reached the active site in each simulation in less than 5 ns (Fig. 2). Taking together the trajectories of all five ELS simulations (250-ns total), a total of 148 $O_2$ molecules reached the active site, averaging to one per 1.7 ns. Of these 148 events, 26 are cases where the same $O_2$ molecule had two or more entries, since the simulation allowed molecules to diffuse back into the solution and return. The data are summarized in Table 1. The density map of $O_2$ within the protein was determined by combining the last 40 ns segments of the five simulations, and was normalized with respect to the average $O_2$ density in the aqueous phase. The results are displayed as a 3D isosurface image (Fig. 3) in order to facilitate comparison to the ILS results (Fig. 4).

The ELS simulations reveal high-occupancy regions within the protein which form a Y-shaped $O_2$ pathway with two openings at the protein interface with lipids, pathways leading from these openings (Branches A and B, Fig. 3a) to a common branch-point, and a single pathway leading from the branch-point to the active site. The branch-point is surrounded by residues I78, A149 and L200 (Fig. 3b). The red surfaces in Fig. 3a are isosurfaces where the free energy with respect to the aqueous phase ($\Delta G_{i,sol}$) is −3.5 kcal/mol. This represents favorable partitioning from the aqueous phase to these regions of about 300 folds and a 10-to-50-fold favorable partitioning of $O_2$ with respect to the membrane phase (depending on the location within the membrane). Fig. 3b shows the isosurfaces defining $\Delta G_{i,sol}$ =−3.0 (red-wireframe) and −4.0 kcal/mol (purple-solid), indicating higher and lower $O_2$ affinity sites along the pathway. Examination of all $O_2$ trajectories shows that all the $O_2$ reaching the active site use the Y-shaped pathway shown in Figs. 3a and b. All the $O_2$ comes from the lipid bilayer and through the hydrophobic tunnel to reach the active site (Supp. Fig. 2). Fig. 3c shows that the pathways correspond to the Xe binding sites observed by X-ray crystallography.[35,40] The X-ray Xe binding sites overlap with several purple isosurfaces in Fig. 3b indicating $O_2$ binding sites ($\Delta G_{i,sol}$ =−4.0 kcal/mol).

The ILS calculations result in an energetic picture that is fully in line with ELS simulations, as shown by the free energy isosurfaces in Figs. 4a and b. Additional regions of the protein that favorably bind $O_2$ are also revealed by both the ELS simulations and ILS calculations, but these are isolated cavities that do not constitute a pathway. Fig. 5a shows a 2D-projection of the free energy map, which strongly supports the conclusion that no pathway other than the Y-shaped pathway is available for $O_2$ to reach the enzyme's active site. The Y-shaped pathway has a radius throughout its length of at least 1.5Å (Figs. 4c and d), which is large enough for unhampered diffusion of $O_2$. During the simulations, no protein fluctuations of

blocked or altered the pathways, and the protein structure was not altered by the presence of $O_2$, even at such a high concentration as 210mM (Supp. Fig. 3). The agreement of the ELS and ILS results demonstrates that the 50-ns simulations are sufficiently long for adequate sampling of $O_2$ diffusion throughout the protein.

There are 7 to 8 binding sites of $O_2$ along the Y-shaped pathway (Figs. 3b, 5a and 5b). These sites have $\Delta G_{i,sol}$ values ranging from −3.5 to −4.5 kcal/mol, corresponding to dissociation constants of 0.6 to 3mM. If the concentration is 250 $\mu$M (air saturated), these data predict between 0.5 and 1 $O_2$ present within the pathway. Under more physiologically relevant conditions, the amount of $O_2$ present within the protein at equilibrium will be negligible. Figs. 3 and 5b provide more details relating the Xe binding sites[35,40] to the regions of the protein favorable for $O_2$ binding. The site closest to the active site coincides with Xe1 in the X-ray structure (Figs. 3b and 3c[35] ). The affinity for $O_2$ at the branch-point (BP) is most favorable and corresponds to the combination of Xe5 and Xe6 densities in the X-ray structure.[35] The two $O_2$ sites in Branch B coincide with Xe3 and Xe4. Branch A contains 3 $O_2$ binding sites. Two are located near the entrance of Branch A (residues V79 and A120) and are not visualized by X-ray crystallography. The third $O_2$ site in Branch A coincides with the region around Xe2 and Xe7. The 1D-projection free energy profiles of $O_2$ in Fig. 5c show the largest free-energy barrier along the Y-shaped pathway of only 1.5 kcal/mol, located at the transition from the BP to the Xe1 site, which is very close to the active site. Other free-energy barriers are all below 1 kcal/mol.

### The rate of delivery of $O_2$ to the active site

To obtain an estimate of the rate of $O_2$ delivery to the active site, a series of 21 short ELS simulations (3–5 ns each) were performed to determine the time required for the first $O_2$ from the solution to reach the active site. This was defined arbitrarily as an $O_2$ molecule getting to within 6Å of $Cu_B$. The initial distribution of $O_2$ was 90 molecules in the membrane and 10 molecules in the aqueous phase, which is equivalent to an $O_2$ concentration of 37mM in the aqueous phase and 185mM in the membrane. Similar to the 50-ns ELS simulations, $O_2$ molecules were initially placed outside the protein in these short ELS simulations. In all 21 trials, $O_2$ diffused to the active site within the first 5 ns. In 14 trials, $O_2$ reaching the active site entered via Branch B and in the remaining 7 trials, through Branch A (Table 2). On the average, it took 1.7 ns for $O_2$ to diffuse to the immediate vicinity of $Cu_B$, essentially the same as observed in the 50-ns ELS simulations. Using the nominal concentration in the aqueous phase (37 mM), we may estimate an apparent second order rate constant of $(1/0.037\text{M})(1/1.7\times10^{-9}\text{s})=1.6\times10^{10}\ \text{M}^{-1}\text{s}^{-1}$. This is an “apparent” second order rate constant since the $O_2$ molecules that reach the active site are initially within the membrane and then must pass through the protein tunnel. The apparent rate constant has been experimentally determined to be $1\times10^{9}\ \text{M}^{-1}\text{s}^{-1}$ by determining the rate of formation of the initial $O_2$ adduct with heme $a_3$, using enzymes dissolved in detergent micelles.[42] The important point is that the calculated estimate is consistent with a remarkably rapid rate of diffusion of $O_2$ to reach the active site.

Further insight is obtained by observing transit times for successful trajectories of $O_2$ for the molecule to reach the entrance of either Branch A or B, and the transit from the pathway’s

entrance(s) to $Cu_B$ (Table 2). The average time for $O_2$ (at 37mM) to get into the entrance of the pathway (either branch) is about $t_{out \rightarrow ent} \approx 1$ ns. Once at the entrance of the pathway, the average transit time to the active site ($Cu_B$) is $t_{ent \rightarrow cat} \approx 0.6 \pm 0.4$ ns. All the successful trajectories took $O_2$ to the BP ($t_{ent \rightarrow BP} \approx 0.2$ ns) and to $Cu_B$ ($t_{BP \rightarrow cat} \approx 0.4$ ns). The fraction of $O_2$ molecules that started at the entrance of either Branch A or B and the went on the reach $Cu_B$ is about 40 %. It should be noted that the time for $O_2$ to diffuse to the entrance of the pathway will depend inversely on $O_2$ concentration in the membrane, but the transit times within the $O_2$ pathway and the fraction of molecules that reach the active site once entering the pathway will be independent of $O_2$ concentration.

### *In silico* mutagenesis of the $O_2$ pathway

Seven different mutants were constructed *in silico* to determine their influence on the diffusion of $O_2$ through the Y-shaped pathway (Table 3). In each of these mutants, the native residues were replaced by a bulky side chain, namely phenylalanine or tryptophan. These residues are I78, A149, A120, S150, V79 and L200, which correspond to F67, L150, H151, L112, F68 and L202 of the bovine cytochrome c oxidase or F108, V194, A153, H195, F109 and L246 of the *R. sphaeroides* enzyme.

1. I78F (Fig. 6 and Supp. Fig. 4): Although I78 is at the BP, its replacement by phenylalanine has only a modest effect on the free energy barrier of $O_2$ translocation along the pathway.
2. A149F (Figs. 6 and 8, and Supp. Figs. 4 and 5): A149 is located at the BP. Although its replacement by phenylalanine creates a barrier, $O_2$ can readily bypass it and still reach the active site via both Branches A and B. Short ELS simulations show that this mutation has only a modest effect on the transit time of $O_2$ to the active site.
3. A120F (Figs. 6 and 8, and Supp. Figs. 4 and 5): A120 is located within Branch A and the X-ray structure of the A120F mutant has been reported.[31] Although the structure of this mutant perfectly aligns with the wild-type structure, the introduced phenylalanine at this position occupies the Xe2–Xe7 sites, as shown both in the X-ray structure[31] and in the simulation (Fig. 6), and reduces $O_2$ diffusion through branch A. However, since Branch B is still fully functional, the net effect on the rate of $O_2$ diffusion to the active site is modest.
4. S150W (Figs. 6 and 8, and Supp. Figs. 4 and 5): S150 is at the entrance of Branch B. A tryptophan at this position creates a significant barrier to $O_2$ diffusion and reduces the radius of the pathway to below 1.2Å. However, Branch A is still fully functional, and the time required for $O_2$ to reach the active site is only modestly influenced.
5. A120F/S150W double mutant (Figs. 7 and 8, and Supp. Figs. 5 and 6): Ten simulations (5–10 ns each) were performed for this mutant, and $O_2$ was observed to reach the active site in eight of them. This mutant increases the barrier to $O_2$ diffusion through both Branches A and B, but

the net result is only to double the average time required for the first $O_2$ to reach the active site during the simulations (Table 3).

6. V79F/S150W double mutant (Figs. 7 and 8, and Supp. Figs. 5 and 6): V79 is located at the entrance of Branch A, near A120. This double mutant also increases the barrier against $O_2$ diffusion through both Branches A and B. However, in 18 of 20 simulations (5–10 ns each), $O_2$ reached the active site and the time for the first $O_2$ was only increased by a factor of 2.

7. I78F/V79F/L200F triple mutant (Figs. 7 and 8, and Supp. Figs. 5 and 6): L200 is located near S150 at the entrance of Branch B. This triple mutant increases barriers to $O_2$ diffusion at the BP as well as the entrances of each branch. A total of 30 simulations ranging from 5 to 15 ns were performed and in 29 of these $O_2$ reached the active site. The time required for the first $O_2$ to reach the active site is about 4-fold greater than in the wild type (6.7 ns vs. 1.7 ns).

Hence, the expectation for these mutations is that the effects on the transit of $O_2$ through the protein will be modest. We note that the length of the simulations performed here may not be sufficient to detect potentially large conformational changes, beyond the observed local constrictions of the $O_2$ pathway described above. However, we also note that the crystal structures of different types of cytochrome oxidases in which the regions studied here by in silico mutagenesis show variations in their amino acid compositions, have indicated no global structural differences. Furthermore, a crystal structure of one of the mutants studied here (A120F)[31] perfectly aligns with the wild-type structure. Based on these, we do not expect significant global structural changes in the enzyme due to the introduced mutations.

## Discussion

This study is motivated by the report of the remarkably fast rate of $O_2$ diffusion into the deeply buried active site of cytochrome $ba_3$ for *T. thermophilus* The experimentally determined second order rate constant at 298K for the formation of the initial complex of $O_2$ with the active-site heme $a_3$ is $k^1 = 1 \times 10^9$ $M^{-1}s^{-1}$.[42,43] This is ten times faster than the rate constant for the equivalent first step in the reaction of the mitochondrial cytochrome c oxidase, $k^1 = 1 \times 10^8$ $M^{-1}s^{-1}$,[42,43] 100 times faster than $O_2$ binding to myoglobin, $k^1 = 1.6 \times 10^7$ $M^{-1}s^{-1}$,[75] and 100 times larger than $O_2$ diffusing into the diiron active site of toluene/oxylene monooxygenase hydroxylase, $k^1 = 2.1 \times 10^5$ $M^{-1}s^{-1}$.[76] The rate constant for CO or $O_2$ to reach the buried active site of NiFe hydrogenase has been measured to be $6.3 \times 10^7$ $M^{-1}s^{-1}$,[77] also considerably less than cytochrome $ba_3$.

The first experiments to measure the diffusion of $O_2$ within proteins determined the rate constant for the collisional quenching by $O_2$ of the fluorescence of tryptophan within small soluble proteins.[78,79] The second order rate constants for this were found to be diffusion-limited, in the range of $2–8 \times 10^9$ $M^{-1}s^{-1}$. Residues internally buried within the proteins that are not accessible to $O_2$ based on the static X-ray structures were readily quenched by collisional contact with $O_2$. It was estimated that $O_2$ could diffuse through the protein at rates that are 20–50% of the diffusion rate in water,[79] providing one of the first

demonstrations of protein dynamics, necessary to allow $O_2$ to penetrate the protein. Although these data suggest that there may be no need for specific pathways to facilitate the diffusion of $O_2$ or other small, hydrophobic gases within proteins, considerable experimental and computational evidence indicates that such pathways have evolved for enzymes that use small gas molecules as substrates, e.g., nitrogenase,[80] methane monooxygenase,[81,82] laccase,[83,84] NiFe hydrogenase,[77,85] FeFe hydrogenase,[36,86] D-amino acid oxidase,[67] copper amine oxidase, [87] myoglobin,[45,75,88–90] hemoglobin,[91] CO dehydrogenase/acetyl-CoA synthase,[92] and heme-copper oxygen reductases, including cytochrome $ba_3$.[33–35,40–43,58,93–95] There are also several examples of enzymes with multiple active sites that have molecular tunnels for delivering the product generated at one site to a second distant site where it is consumed as a substrate.[15]

In many cases, the gas channels include hydrophobic cavities that are identified by locating Xe binding sites using X-ray crystallography.[36] An important caveat is that the Xe binding sites identified crystallographically may not be functional and need not be involved in $O_2$ diffusion within the protein. For example, photosystem II from *Thermosynechococcus elongates* [96] has 25 Xe binding sites scattered through the membrane domain of the protein, but they are clearly not involved in $O_2$ diffusion away from the oxygen evolving cluster. Myoglobin has 4 Xe binding sites, which may also bind $O_2$, but it remains unclear which, if any, of these sites are on the primary pathway for $O_2$ to reach the heme Fe.[75,90]

Protein conformational changes are often crucial either in the transient formation of the hydrophobic cavities or in opening the passage connecting adjacent hydrophobic cavities, thus allowing passage of $O_2$. These are dynamic tunnels. An example of this is the pathway for $CO_2$ to reach the buried metal cluster where it is reduced to CO in the CO dehydrogenase/acetyl-CoA synthase.[92] Dynamic tunnels have also been proposed for FeFe hydrogenase,[36,86] the *Scarpharca* dimeric hemoglobin,[91] laccase,[84] and for the HCO from *R. sphaeroides*.[41]

A recent MD study in the cytochrome c oxidase from *R. sphaeroides* [41] concluded that the X-ray inferred tunnel is not an important route for $O_2$ to reach the active site and are in contrast with the finding reported here on cytochrome $ba_3$. The HCO from *R. sphaeroides* is an A-family heme-copper oxygen reductase, and crystallographic studies previously identified a putative $O_2$ pathway with two Xe binding sites.[29] This tunnel is roughly in the same location as the tunnel observed here in cytochrome $ba_3$, which is a B-family HCO. The functionality of the X-ray inferred tunnel in two different A-family heme-copper oxygen reductases has been tested experimentally by site-directed mutations.[94,97,98] However, these mutations are too close to the active site to allow straightforward interpretation. Using computational techniques similar to those employed in the present study, three putative $O_2$ pathways were suggested in the *R. sphaeroides* HCO,[41] one corresponding to that inferred by the X-ray studies. A detailed examination of the structures of the A-family HCOs[33] as well as the MD simulations[41] have revealed a constriction in the X-ray inferred tunnel that would substantially impede the passage of $O_2$ molecules to the active site. MD simulations did not observe any delivery event of $O_2$ to the active site over 100-ns periods.[41] Nevertheless, free-energy profiles estimated from data generated by ILS calculations suggested two probable alternative pathways for $O_2$ diffusion from the solvent to the active

site.[41] Since the free-energy barriers of the two pathways were estimated to be 5 kcal/mol lower than the X-ray inferred tunnel, it was concluded that these alternative pathways, not observed in the static X-ray structures, are the preferred routes used in the *R. sphaeroides* HCO.[41]

In contrast, the inferred pathway from X-ray data for $O_2$ diffusion to the active site of cytochrome $ba_3$ is supported by both previous experimental data and by MD simulations, which only concentrated on the dynamics and stability of $O_2$ binding at individual X-ray Xe sites,[33,34] as well as the present study. The tunnel in this B-family heme-copper oxygen reductase does not have the constriction observed in the A-family enzymes.[33,35] The constriction in the A-family HCOs is due to bulky residues W172 and F282 (numbering for the *R. sphaeroides enzyme*) or residues W126 and F238 (numbering for the bovine enzyme), whereas the equivalent residues in the *T. thermophilus* enzyme are Y133 and T231. The examination of the Y133W mutant of cytochrome $ba_3$ showed that the second order rate constant for $O_2$ to diffuse to the active site is slowed down 5-fold to $k_1 = 2\times10^8$ $M^{-1}s^{-1}$.[33] Short (1 ns) MD simulations showed that there is effectively no barrier within this tunnel for $O_2$ diffusion.[34]

The present study employs long ELS MD simulations (50 ns) with a model that places the entire 3-subunit cytochrome $ba_3$ in a lipid bilayer surrounded by an aqueous solution. By initially placing $O_2$ molecules outside the protein, this allows not only substrate $O_2$ to unequivocally search for its delivery pathways, but also to address the role of protein dynamics in modulating the X-ray inferred tunnel and to forming other alternative pathways. A sufficient number of trajectories were obtained for $O_2$, starting outside the protein and reaching the active site, to estimate a free energy map of $O_2$ within the protein based on occupancy. In addition, ILS calculations were performed to obtain an independent free energy map of $O_2$ in the protein. The results of both the ELS and ILS calculations are in full agreement with each other as well as previous experimental and computational studies.[33,34] The most important points are summarized below.

1. The equilibrium distribution of $O_2$ between the membrane and aqueous phases, as well as distribution of $O_2$ within the membrane in the computational model are consistent with previous experimental and computational data.[73,74]

2. The protein contains about 7 binding sites for $O_2$ corresponding generally to the Xe binding sites in the X-ray structure. At 298 K, each site has a dissociation constant for $O_2$ of about 1mM with respect to the concentration in aqueous solution. At 250 $\mu$M $O_2$, at equilibrium there will be an average of about 1 $O_2$ molecule present in the protein, distributed among the sites within the pathway. At 10 $\mu$M $O_2$, more realistic physiologically, the occupancy of each site is less than 1% (at 298 K). Hence, these binding sites do not act as a storage reservoir for $O_2$.

3. The average time for $O_2$ to reach an entrance of its delivery pathway is about 1 ns, starting with a concentration of 37mM in the aqueous phase (MD simulation condition). The first $O_2$ molecule to reach the pathway

entrance in each simulation always originates in the lipid bilayer. Based on the concentration of $O_2$ in solution, the apparent second order rate constant to reach the pathway entrance is about $1.6\times10^{10}$ $M^{-1}s^{-1}$. This compares favorably with the measured second order rate constant for the collisional quenching by $O_2$ of pyrene dissolved in the lipid bilayer of $1.2\times10^{10}$ $M^{-1}s^{-1}$.[99] When the dissolved $O_2$ concentration in the aqueous phase is 250 $\mu$M (air saturated water at 298 K), the rate for an $O_2$ molecule to reach the pathway entrance can be estimated to be $(2.5\times10^{-4}$ M) $(1.6\times10^{10}$ $M^{-1}s^{-1})=4\times10^{6}$ $s^{-1}$, or about one $O_2$ per 250 ns.

4. The $O_2$ binding sites right next to the pathway entrances have binding free energies of about −1.5 to −2 kcal/mol with respect to the $O_2$ pool within the membrane, recalling that $O_2$ in the lipid is favored by about −2 kcal/mol with respect to $O_2$ in solution. This is equivalent to an association constant of about 20 for $O_2$ binding from the lipid bilayer. Since the simulated second order rate constant to reach these sites from the bilayer is $1.6\times10^{10}$ $M^{-1}s^{-1}$, the off rate constant can be estimated to be $k_{-1}$ $=(1.6\times10^{10}/20)=8\times10^{8}$ $s^{-1}$. The transit time from the pathway entrance to the active site is 0.6 ns, so the first order rate constant to transit through the pathway is $k_2$ $=(1/6\times10^{-10})=1.7\times10^{9}$ $s^{-1}$. These rough estimates indicate that about half the molecules that get into the pathway make it all the way to the active site. At no point do protein conformational changes introduce any significant free energy barrier to the diffusion of $O_2$ within the delivery pathway.

5. We can model the steady state kinetics of collision with the active site as a two-step process: i) a reversible step to enter the pathway from the lipid, followed by ii) an irreversible step to reach the active site. The $O_2$ that reaches the active site is assumed in this model to be consumed with 100% efficiency.

$$[O_2]+E \underset{k_{-1}}{\overset{[S]k_1}{\rightleftharpoons}} E(O_2) \xrightarrow{k_2} E(O_2)_{Cu_B}$$

The observed rate for $O_2$ reaching the active site in this model is given by

$$k_{obs}=\frac{[O_2]k_1k_2}{[O_2]k_1+k_{-1}+k_2}$$

For any reasonable value of $[O_2]$, it is reasonable to assume $[O_2]k_1 \ll k_{-1}$, $k_2$. Then

$$k_{obs} \approx \frac{[O_2]k_1k_2}{k_{-1}+k_2} \approx 1.5\times10^{10}[O_2]\,s^{-1}$$

assuming $k_1$ =1.6×10$^{10}$ M$^{-1}$s$^{-1}$, $k_{-1}$ =8×10$^8$ s$^{-1}$ and $k_2$ =1.7×10$^{10}$ s$^{-1}$. The second order rate constant for $O_2$ to reach the active site is predicted to be about 1.5×10$^{10}$ M$^{-1}$s$^{-1}$, which is about 15-fold larger than the measured rate constant of 1×10$^9$ M$^{-1}$s$^{-1}$.[42] The experimental measure of the second order rate constant includes the process of forming the adduct with heme $a_3$ at the active site, and this could be rate-limiting, explaining why the value is smaller than the rate of reaching the vicinity of the active site which is computed. In any event, the MD simulations demonstrate that diffusion through the body of the protein is not rate limiting.

6. In order for the rate of transit through the protein to be rate limiting, it would be necessary to slow the transit time to about 100 ns or $k_2$ =10$^7$s$^{-1}$. This would mean adding about 3 kcal/mol to the highest energy barrier (to 4.5 kcal/mol), and would result in a second order rate constant of about 10$^8$ M$^{-1}$s$^{-1}$, which is what is measured for the bovine cytochrome c oxidase and is the result of adding a constriction to the pathway in cytochrome $ba_3$.

7. Using the measured rate constant, 1×10$^{10}$ M$^{-1}$s$^{-1}$, and assuming that the maximum rate of catalysis is $k_{cat}$ ≈10$^2$ s$^{-1}$ $O_2$ reduced /sec, the enzyme will be limited by the dissolved concentration of $O_2$ at concentrations of less than about 10$^{-7}$M (0.1 $\mu$M) at 298 K. At concentrations of $O_2$ greater than 0.1 $\mu$M, the chemistry of catalysis is rate limiting.

8. In the native enzyme, the highest free energy barrier is about 1.5 kcal/mol. Mutations in the pathway that slow the rate of $O_2$ diffusion through the protein must present a free energy barrier of at least 4 kcal/mol, which would lower the second order rate constant to about 10$^8$ M$^{-1}$s$^{-1}$, which is what the Y133W must accomplish in cytochrome $ba_3$.[33]

9. If the second order rate constant for $O_2$ to reach the active site were reduced to 10$^7$ M$^{-1}$s$^{-1}$, similar to the value for myoglobin, the consequence would be that the concentration of $O_2$ would limit the turnover rate of the enzyme at 10 $\mu$M instead of 0.1 $\mu$M. This is in a range that is physiologically significant, and provides a plausible rationale for why the respiratory HCOs have evolved to allow very fast access to the enzyme's active site. The unusual hydrophobic tunnel present in cytochrome $ba_3$ with a largest free energy barrier of 1.5 kcal/mol suggests that this enzyme has evolved for maximum turnover even at concentrations of its $O_2$ substrate down to 0.1 $\mu$M. It is noted that this enzyme from *T. thermophilus* normally functions at 75°C or 348 K, so conclusions about physiological relevance involve extrapolations from the simulations and experiments done at or near 25°C (298 K).

In summary, a combination of ELS MD simulations and ILS thermodynamic calculations provide a consistent explanation for the rapid kinetics of $O_2$ to access the active site of cytochrome $ba_3$: the protein has a hydrophobic, static tunnel that provides an unencumbered

25-Å pathway from the lipid bilayer to the active site, allowing the enzyme to operate at maximal velocity at $O_2$ concentrations as low as 0.1 $\mu$M at 298 K.

## Acknowledgments

The authors acknowledge supercomputing resources at National Science Foundation Supercomputing Centers (XSEDE MCA06N060) and funding from the National Institutes of Health (NIH P41-GM104601 and U01-GM111251 to E.T., and R01-HL16101 to R.B.G.). P.M. gratefully acknowledges NIH support as a trainee of the Molecular Biophysics Training Program (5T32-GM008276).

## Abbreviations

| | |
|---|---|
| **HCO** | heme-copper oxygen reductase |
| **$ba_3$** | cytochrome $ba_3$ oxidase |
| **ELS** | explicit ligand sampling |
| **ILS** | implicit ligand sampling |

## References

1. Wikström M. Active site intermediates in the reactions of $O_2$ by cytochrome oxidase, and their derivatives. Biochim Biophys Acta – Bioener. 2012; 1817:468–475.
2. Wikström M, Verkhovsky MI. Mechanism and energetics for proton translocation by the respiratory heme-copper oxidases. Biochim Biophys Acta – Bioener. 2007; 1767:1200–1214.
3. Hosler JP, Ferguson-Miller S, Mills DA. Energy transduction: proton transfer through the respiratory complexes. Annu Rev Biochem. 2006; 75:165–187. [PubMed: 16756489]
4. Kaila VR, Verkhovsky MI, Wikström M. Proton-coupled electron transfer in cytochrome oxidase. Chem Rev. 2010; 110:7062–7082. [PubMed: 21053971]
5. Sousa FL, Alves RJ, Ribeiro MA, Pereira-Leal JB, Teixeira M, Pereira MM. The superfamily of heme-copper oxygen reductases: Types and evolutionary considerations. Biochim Biophys Acta – Bioener. 2012; 1817:629–637.
6. Brzezinski P, Gennis RB. Cytochrome c oxidase: exciting progress and remaining mysteries. J Bioenerg Biomembr. 2008; 40:521–531. [PubMed: 18975062]
7. Ferguson-Miller S, Hiser C, Liu J. Gating and regulation of the cytochrome c oxidase proton pump. Biochim Biophys Acta – Bioener. 2012; 1817:489–494.
8. Belevich L, Bloch DA, Belevich N, Wikström M, Verkhovsky MI. Exploring the proton pump mechanism of cytochrome c oxidase in real time. Proc Natl Acad Sci USA. 2007; 104:2685–2690. [PubMed: 17293458]
9. Belevich L, Verkhovsky MI, Wikström M. Proton-coupled electron transfer drives the proton pump of cytochrome c oxidase. Nature. 2006; 440:829–832. [PubMed: 16598262]
10. Sharma V, Wikström M. A structural and functional perspective on the evolution of the heme-copper oxidases. FEBS Lett. 2014; 588:3787–3792. [PubMed: 25261254]
11. Hemp J, Gennis RB. Diversity of the Heme-Copper superfamily in Archaea: Insights from Genomics and Structural Modeling. Results Probl Cell Differ. 2008; 45:1–31. [PubMed: 18183358]
12. Brochier-Armanet C, Talla E, Gribaldo S. The multiple evolutionary histories of dioxygen reductases: Implications for the origin and evolution of aerobic respiration. Mol Biol Evol. 2009; 26:285–297. [PubMed: 18974088]
13. Ducluzeau AL, Schoepp-Cothenet B, van Lis R, Baymann F, Russell MJ, Nitschke W. The evolution of respiratory $O_2$/NO reductases: an out-of-the-phylogenetic-box perspective. J R Soc Interface. 2014; 11:20140196. [PubMed: 24968694]

14. Huang X, Holden HM, Raushel FM. Channeling of substrates and intermediates in enzyme-catalyzed reactions. Arch Phys Biochem. 2001; 70:149–180.
15. Raushel FM, Thoden JB, Holden HM. Enzymes with molecular tunnels. Acc Chem Res. 2003; 36:539–548. [PubMed: 12859215]
16. Thoden JB, Huang X, Raushel FM, Holden HM. Carbamoyl-phosphate synthethase. Creation of an escape route for ammonia. J Biol Chem. 2002; 277:39722–39727. [PubMed: 12130656]
17. Huang HX, McCammon A. The gates of ion channels and enzymes. Trends Biochem Sci. 2010; 35:179–185. [PubMed: 19926290]
18. Gora A, Brezovsky J, Damborsky J. Gates of enzymes. Chem Rev. 2013; 113:5871–5923. [PubMed: 23617803]
19. Shaikh SA, Li J, Enkavi G, Wen PC, Huang Z, Tajkhorshid E. Visualizing functional motions of membrane transporters with molecular dynamics simulations. Biochemistry. 2013; 52:569–587. [PubMed: 23298176]
20. Henzler-Wildman K, Kern D. Dynamic personalities of proteins. Nature. 2007; 450:964–972. [PubMed: 18075575]
21. Ferguson-Miller S, Babcock G. Heme/Copper terminal oxidases. Chem Rev. 1996; 96:2889–2907. [PubMed: 11848844]
22. Sharpe, MA.; Qin, L.; Ferguson-Miller, S. From Biophysical and Structural Aspects of Bioenergetics. In: Wikström, M., editor. Methods in Molecular Biology. RSC Publishing; Cambridge, UK: 2005. p. 26-54.
23. Han H, Hemp J, Pace LA, Ouyang H, Ganesan K, Roh JH, Daldal F, Blanke SR, Gennis RB. Adaptation of aerobic respiration to low $O_2$ environments. Proc Natl Acad Sci USA. 2011; 108:14109–14114. [PubMed: 21844375]
24. Agmon N. The Grotthuss mechanism. Chem Phys Lett. 1995; 244:456–462.
25. Yamashita T, Voth GA. Insights into the mechanism of proton transport in cytochrome c oxidase. J Am Chem Soc. 2011; 134:1147–1152.
26. Iwata S, Ostermeier C, Ludwig B, Michel H. Structure at 2.8Å Resolution of Cytochrome *C* Oxidase From *Paracoccus denitrificans*. Nature. 1995; 376:660–669. [PubMed: 7651515]
27. Tsukihara T, Aoyama H, Yamashita E, Tomizaki T, Yamaguchi H, Shinnzawha-Itoh K, Nakashima R, Yaono R, Yoshikawa S. Structures of Metal Sites of Oxidized Bovine Heart Cytochrome C Oxidase at 2.8Å. Science. 1995; 269:1069–1074. [PubMed: 7652554]
28. Soulimane T, Buse G, Bourenkov GP, Bartunik HD, Huber R, Than ME. Structure and mechanism of the abberrant $ba_3$-cytochrome c oxidase from *Thermus thermophilus*. EMBO J. 2000; 19:1766–1776. [PubMed: 10775261]
29. Svensson-Ek M, Abramson J, Larsson G, Törnroth S, Brzezinski P, Iwata S. The X-ray Crystal Structures of Wild-type and EQ(I–286) Mutant Cytochrome c Oxidases from *Rhodobacter sphaeroides*. J Mol Biol. 2002; 321:329–339. [PubMed: 12144789]
30. Shinzawa-Itoh K, Aoyama H, Muramoto K, Terada H, Kurauchi T, Tadehara Y, Yamasaki A, Sugimura T, Kurono S, Tsujimoto K, Mizushima T, Yamashita E, Tsukihara T, Yoshikawa S. Structures and physiological roles of 13 integral lipids of bovine heart cytochrome c oxidase. EMBO J. 2007; 26:1713–1725. [PubMed: 17332748]
31. Tiefenbrunn T, Liu W, Chen Y, Katritch V, Stout CD, Fee JA, Cherezov V. High Resolution Structure of the $ba_3$ Cytochrome c Oxidase from *Thermus thermophilus* in a Lipidic Environment. PLoS One. 2011; 6:e22348. [PubMed: 21814577]
32. Lyons JA, Aragao D, Slattery O, Pisliakov AV, Soulimane T, Caffrey M. Structural insights into electron transfer in $caa_3$-type cytochrome oxidase. Nature. 2012; 487:514–518. [PubMed: 22763450]
33. McDonald W, Funatogawa C, Li Y, Szundi I, Fee YCJA, Stout CD, Einarsdóttir O. Ligand access to the active site in *Thermus thermophilus* $ba_3$ and bovine heart $aa_3$ cytochrome oxidases. Biochemistry. 2013; 52:640–652. [PubMed: 23282175]
34. McDonald W, Funatogawa C, Li Y, Chen Y, Szundi I, Fee JA, Stout CD, Einarsdóttir O. Conserved Glycine 232 in the Ligand Channel of $ba_3$ cytochrome oxidase of *Thermus thermophilus*. Biochemistry. 2014; 53:4467–4475. [PubMed: 24937405]

35. Luna VM, Chen Y, Fee JA, Stout CD. Crystallographic stuides of Xe and Kr binding within the large internal cavity of cytochrome $ba_3$ from *Thermus thermophilus*: structural analysis and role of oxygen transport channels in the heme-Cu oxidases. Biochemistry. 2008; 47:4657–4665. [PubMed: 18376849]
36. Lautier T, Ezanno P, Baffert C, Fourmond V, Cournac L, Fontecilla-Camps JC, Soucaille P, Bertrand P, Meyinal-Salles I, Léger C. The quest for a functional substrate access tunnel in FeFe hydrogenase. Faraday Discuss. 2011; 148:385–407. [PubMed: 21322495]
37. Doukov TI, Blasiak LC, Servalli J, Ragsdale SW, Drennan CL. Xenon in and at the end of the tunnel of bifunctional carbon monoxide dehydrogenase/acetyl-CoA synthase. Biochemistry. 2008; 47:3474–3483. [PubMed: 18293927]
38. McCormick MS, Lippard SJ. Analysis of substrate access to active sites in bacterial multicomponent monooxygenase hydroxylase: X-ray crystal structure of Xenon-pressurized phenol hydroxylase from *Pseudomonas* sp. OX1. Biochemistry. 2011; 50:11058–11069. [PubMed: 22136180]
39. Brunori M, Gibson QH. Cavities and packing defects in the structural dynamics of myoglobin. EMBO Rep. 2001; 2:676–679.
40. Luna VM, Fee JA, Deniz AA, Stout CD. Mobility of Xe Atoms within the Oxygen Diffusion Channel of Cytochrome $ba_3$ oxidase. Biochemistry. 2012; 51:4669–4676. [PubMed: 22607023]
41. Oliveira AS, Damas JM, Baptista A, Soares CM. Exploring $O_2$ diffusion in A-type cytochrome c oxidases: molecular dynamics simulations uncover two alternative channels towards the binuclear site. PLoS Comput Biol. 2011; 10:e1004010.
42. Szundi I, Funatogawa C, Fee JA, Soulimane T, Einarsdóttir O. CO impedes superfast $O_2$ binding in $ba_3$ cytochrome oxidase from *Thermus thermophilus*. Proc Natl Acad Sci USA. 2010; 107:21010–21015. [PubMed: 21097703]
43. Einarsdóttir O, Funatogawa C, Soulimane T, Szundi I. Kinetic studies of the reactions of $O_2$ and NO with reduced *Thermus thermophilus* $ba_3$ and bovine $aa_3$ using photolabile carriers. Biochim Biophys Acta – Bioener. 2012; 1817:672–679.
44. Olson JS, Phillips GN Jr. Myoglobin discriminates between $O_2$, NO, and CO by electrostatic interactions with the bound ligand. J Biol Inorg Chem. 1997; 2:544–552.
45. Cohen J, Arkhipov A, Braun R, Schulten K. Imaging the migration pathways for $O_2$, CO, NO, and Xe inside myoglobin. Biophys J. 2006; 91:1844–1857. [PubMed: 16751246]
46. Hunsicker-Wang L, Pacoma R, Chen Y, Fee J, Stout C. A novel cry-oprotection scheme for enhancing the diffraction of crystals of recombinants cytochrome $ba_3$ oxidase from *Thermus thermophilus*. Acta Cryst D. 2005; 61:340–343. [PubMed: 15735345]
47. Humphrey W, Dalke A, Schulten K. VMD – Visual Molecular Dynamics. J Mol Graphics. 1996; 14:33–38.
48. Phillips JC, Braun R, Wang W, Gumbart J, Tajkhorshid E, Villa E, Chipot C, Skeel RD, Kale L, Schulten K. Scalable Molecular Dynamics with NAMD. J Comp Chem. 2005; 26:1781–1802. [PubMed: 16222654]
49. Ryckaert JP, Ciccotti G, Berendsen HJC. Numerical Integration of the Cartesian Equations of Motion of a System with Constraints: Molecular Dynamics of *n*-Alkanes. J Comp Phys. 1977; 23:327–341.
50. Darden T, York D, Pedersen LG. Particle mesh Ewald: An $N\cdot\log(N)$ method for Ewald sums in large systems. J Chem Phys. 1993; 98:10089–10092.
51. Martyna GJ, Tobias DJ, Klein ML. Constant Pressure Molecular Dynamics Algorithms. J Chem Phys. 1994; 101:4177–4189.
52. Feller SE, Zhang Y, Pastor RW, Brooks BR. Constant pressure molecular dynamics simulation: The Langevin piston method. J Chem Phys. 1995; 103:4613–4621.
53. MacKerell AD Jr, et al. All-atom empirical potential for molecular modeling and dynamics studies of proteins. J Phys Chem B. 1998; 102:3586–3616. [PubMed: 24889800]
54. MacKerell AD Jr, Feig M, Brooks CL III. Extending the Treatment of Backbone Energetics in Protein Force Fields: Limitations of Gas-Phase Quantum Mechanics in Reproducing Protein Conformational Distributions in Molecular Dynamics Simulations. J Comp Chem. 2004; 25:1400–1415. [PubMed: 15185334]

55. Klauda JB, Venable RM, Freites JA, O'Connor JW, Tobias DJ, Mondragon-Ramirez C, Vorobyov I, MacKerell AD Jr, Pastor RW. Update of the CHARMM all-atom additive force field for lipids: Validation on six lipid types. J Phys Chem B. 2010; 114:7830–7843. [PubMed: 20496934]
56. Jorgensen WL, Chandrasekhar J, Madura JD, Impey RW, Klein ML. Comparison of simple potential functions for simulating liquid water. J Chem Phys. 1983; 79:926–935.
57. Vanommeslaeghe K, Hatcher E, Acharya C, Kundu S, Zhong S, Shim J, Darian E, Guvench O, Lopes P, Vorobyov I, MacKerell AD Jr. CHARMM General Force Field: A Force Field for Drug-Like Molecules Compatible with the CHARMM All-Atom Additive Biological Force Fields. J Comp Chem. 2010; 31:671–690. [PubMed: 19575467]
58. Hofacker I, Schulten K. Oxygen and Proton Pathways in Cytochrome *c* Oxidase. Proteins: Struct, Func, Gen. 1998; 30:100–107.
59. Hemp J, Christian C, Barquera B, Gennis RB, Martinez TJ. Helix switching of a key active-site residue in the cytochrome $cbb_3$ oxidases. Biochemistry. 2005; 44:10766–10775. [PubMed: 16086579]
60. Yaffe E, Fishelovitch D, Wolfson HJ, Halperin D, Nussinov R. MolAxis: efficient and accurate identification of channels in macromolecules. PROTEINS: Structure, Function, and Bioinformatics. 2008; 73:72–86.
61. Baylon JL, Lenov IL, Sligar SG, Tajkhorshid E. Characterizing the Membrane-Bound State of Cytochrome P450 3A4: Structure, Depth of Insertion, and Orientation. J Am Chem Soc. 2013; 135:8542–8551. [PubMed: 23697766]
62. Hong G, Pachter R. Inhibition of Biocatalysis in [Fe-Fe] Hydrogenase by Oxygen: Molecular Dynamics and Density Functional Theory Calculations. ACS Chem Biol. 2012; 7:1268–1275. [PubMed: 22563793]
63. Brannigan G, LeBard DN, Hénin J, Eckenhoff RG, Klein ML. Multiple binding sites for the general anesthetic isoflurane identified in the nicotinic acetylcholine receptor transmembrane domain. Proc Natl Acad Sci USA. 2010; 107:14122–14127. [PubMed: 20660787]
64. Murali S, Wallner B, Trudell JR, Bertaccini E, Lindahl E. Microsecond simulations indicate that ethanol binds between subunits and could stabilize an open-state model of a glycine receptor. Biophys J. 2011; 100:1642–1650. [PubMed: 21463577]
65. Wang Y, Cohen J, Boron WF, Schulten K, Tajkhorshid E. Exploring Gas Permeability of Cellular Membranes and Membrane Channels with Molecular Dynamics. J Struct Biol. 2007; 157:534–544. [PubMed: 17306562]
66. Saam J, Ivanov I, Walther M, Holzhutter H, Kuhn H. Molecular dioxygen enters the active site of 12/15 lipoxygenase via dynamic oxygen access channels. Proc Natl Acad Sci USA. 2007; 104:13319–13324. [PubMed: 17675410]
67. Saam J, Rosini E, Molla G, Schulten K, Pollegioni L, Ghisla S. $O_2$-reactivity of flavoproteins: Dynamic access of dioxygen to the active site and role of a $H^+$ relay system in D-amino acid oxidase. J Biol Chem. 2010; 285:24439–24446. [PubMed: 20498362]
68. Wang Y, Tajkhorshid E. Nitric oxide conduction by the brain aquaporin AQP4. Proteins: Struct, Func, Bioinf. 2010; 78:661–670.
69. Frenkel, D.; Smit, B. Understanding Molecular Simulation From Algorithms to Applications. Academic Press; California: 2002.
70. Fischkoff S, Vanderkooi J. Oxygen diffusion in biological and artificial membranes determined by the Flurochrome Pyrene. J Gen Physiol. 1975; 65:663–676. [PubMed: 1176942]
71. Moller M, Botti H, Batthyany C, Rubbo H, Radi R, Denicola A. Direct measurement of nitric oxide and oxygen partitioning into liposomes and low density lipoprotein. J Biol Chem. 2005; 280:8850–8854. [PubMed: 15632138]
72. Dzikovski BG, Livshits VA, Marsh D. Oxygen permeation profile in lipid membrane: comparison with transmembrane polarity profile. Biophys J. 2003; 85:1005–1012. [PubMed: 12885647]
73. Marsh D, Dzikovski BG, Livshits VA. Oxygen profiles in membrane. Biophys J. 2006; 90:L49–L51. [PubMed: 16473906]
74. Al-Abdul-Wahid MS, Evanics F, Prosser RS. Dioxygen transmembrane distributions and partitioning thermodynamics in lipid bilayers and micelles. Biochemistry. 2011; 50:3975–3983. [PubMed: 21510612]

75. Scott EE, Gibson QH, Olson JS. Mapping the Pathways for $O_2$ Entry Into and Exit from Myoglobin. J Biol Chem. 2001; 276:5177–5188. [PubMed: 11018046]
76. Song WJ, Gucinski G, Sazinsky MH, Lippard SJ. Tracking a defined route for $O_2$ migration in a dioxygen-activating diiron enzyme. Proc Natl Acad Sci USA. 2011; 108:14795–14800. [PubMed: 21859951]
77. Liebgott PP, et al. Relating diffusion along the substrate tunnel and oxygen sensitivity in hydrogenase. Nat Chem Biol. 2010; 6:63–70. [PubMed: 19966788]
78. Lakowicz JR, Weber G. Quenching of Protein Fluorescence by Oxygen. Detection of Structural Fluctuations in Proteins on the Nanosecond Time Scale. Biochemistry. 1973; 12:4171–4179. [PubMed: 4200894]
79. Lakowicz JR, Weber G. Quenching of Fluorescence by Oxygen: A Probe for Structural Fluctuations in Macromolecules. Biochemistry. 1973; 12:4161–4170. [PubMed: 4795686]
80. Smith D, Danyal K, Raugei S, Seefeldt LC. Substrate channel in nitrogenase revealed by a molecular dynamics approach. Biochemistry. 2014; 53:2278–2285. [PubMed: 24654842]
81. Whittington DA, Rosenzweig AC, Frederick CA, Lippard SJ. Xenon and halogenated alkanes track putative substrate binding cavities in the soluble methane monooxygenase hydroxylase. Biochemistry. 2001; 40:3476–3482. [PubMed: 11297413]
82. Lee SJ, McCormick MS, Lippard SJ, Cho US. Control of substrate access to the active site in methane monooxygenase. Nature. 2013; 494:380–384. [PubMed: 23395959]
83. Kallio JP, Rouvinen J, Kruus K, Hakulinen N. Probing the dioxygen route in Melanocarpus albomyces laccase with pressurized xenon gas. Biochemistry. 2011; 50:4396–4398. [PubMed: 21524088]
84. Damas JM, Baptista A, Soares CM. The pathway for $O_2$ diffusion inside CotA Laccase and possible implications on the multicopper oxidases family. J Chem Theor Comp. 2014; 10:3525–3531.
85. Wang PH, Best RB, Blumberger J. Multiscale Simulation Reveals Multiple Pathways for $H_2$ and $O_2$ transport in a [NiFe]-Hydrogenase. J Am Chem Soc. 2011; 133:3548–3556. [PubMed: 21341658]
86. Cohen J, Kim K, Posewitz M, Ghirardi ML, Schulten K, Seibert M, King P. Molecular dynamics and experimental investigation of $H_2$ and $O_2$ Diffusion in [Fe]-hydrogenase. Biochem Soc Trans. 2005; 33:80–82. [PubMed: 15667271]
87. Johnson BJ, Cohen J, Welford RW, Pearson AR, Schulten K, Klinman JP, Wilmot CM. Exploring Molecular Oxygen Pathways in *Hanseluna Polymorpha* Copper-Containing Amine Oxidase. J Biol Chem. 2007; 282:17767–17776. [PubMed: 17409383]
88. Cohen J, Schulten K. $O_2$ migration pathways are not conserved across proteins of a similar fold. Biophys J. 2007; 93:3591–3600. [PubMed: 17693478]
89. Olson JS, Soman J Jr, GNP. Ligand pathways in myoglobin: a review of Trp cavity mutations. IUBMB Life. 2007; 59:552–562. [PubMed: 17701550]
90. Jiang Y, Kirmizialtin S, Sanchez IC. Dynamic void distribution in myoglobin and five mutants. Sci Rep. 2014; 4:1–9.
91. Knapp JE, Pahl R, Cohen J, Nichols JC, Schulten K, Gibson QH, Šrajer V, WER. Ligand migration and cavities within Scapharca dimeric HbI: Studies by time-resolved crystallography, Xe binding, and computational analysis. Structure. 2009; 17:1494–1504. [PubMed: 19913484]
92. Wang PH, Bruschi M, Gioia LD, Blumberger J. Uncovering a Dynamically Formed Substrate Access Tunnel in Carbon Monoxide Dehydrogenase/Acetyl-CoA Synthase. J Am Chem Soc. 2013; 135:9493–9502. [PubMed: 23713976]
93. Porrini M, Daskalakis V, Farantos SC. Exploring the topography of free energy surfaces and kinetics of cytochrome c oxidases interacting with small ligands. RCS Advances. 2012; 2:5828–5836.
94. Riistama S, Puustinen A, García-Horsman A, Iwata S, Michel H, Wikström M. Channelling of dioxygen into the respiratory enzyme. Biochim Biophys Acta. 1996; 1275:1–4. [PubMed: 8688439]

95. Einarsdóttir O, McDonald W, Funatogawa C, Szundi I, Woodruff WH, Dyer RB. The pathway of $O_2$ to the active site in heme-copper oxidases. Biochim Biophys Acta – Bioener. 2015; 1847:109–118.

96. Murray JW, Maghlaoui K, Kargul J, Sugiura M, Barber J. Analysis of xenon binding to photosystem II by X-ray crystallography. Photosyn Res. 2008; 98:523–527. [PubMed: 18839332]

97. Salomonsson L, Lee A, Gennis RB, Brzezinski P. A single-amino-acid lid renders a gas-tight compartment within a membrane-bound transporter. Proc Natl Acad Sci USA. 2004; 101:11617–11621. [PubMed: 15289603]

98. Riistama S, Puustinen A, Verkhovsky MI, Morgan JE, Wikström M. Binding of $O_2$ and Its Reduction Are Both Retarded by Replacement of Valine 279 by Isoleucine in Cytochrome c Oxidase from *Paracoccus denitrificans*. Biochemistry. 2000; 39:6365–6372. [PubMed: 10828950]

99. Denicola A, Souza JM, Radi R, Lissi E. Nitric oxide diffusion in membranes determined by fluorescence quenching. Arch Biochem Biophys. 1996; 328:208–212. [PubMed: 8638932]

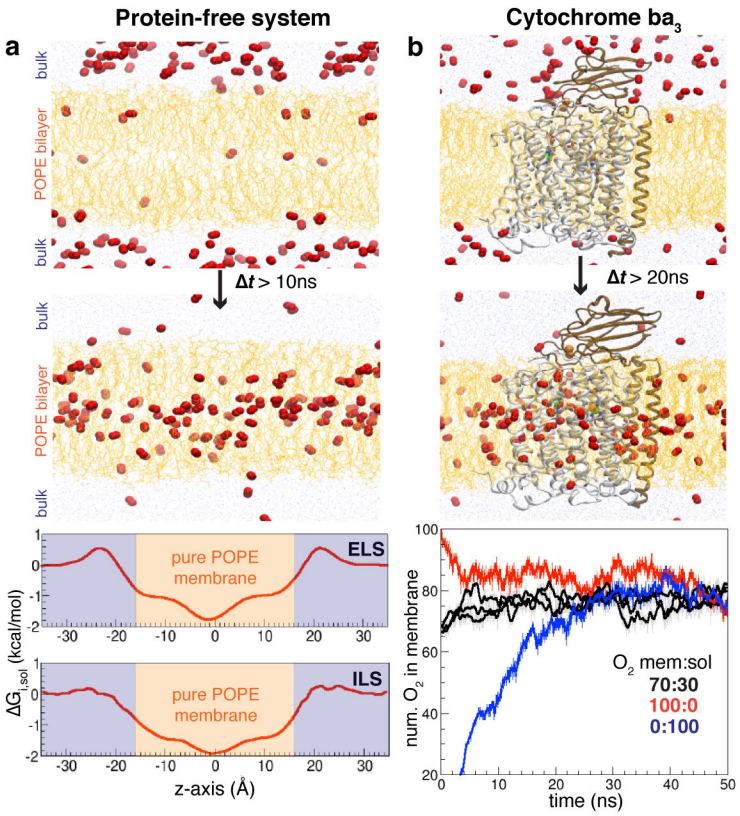


**Figure 1. Partitioning profiles of $O_2$ in membrane**

**a)** Distributions of $O_2$ in membrane vs. aqueous phase in the protein-free system. Top panel illustrates the diffusion of $O_2$ molecules (shown as red balls) from the aqueous phase to the membrane. $O_2$ is considered to be in the membrane when either oxygen atom in the molecule is in between the C22 atoms ($C_\alpha$ of the palmitate's ester) of the POPE lipids in the two leaflets ($-16Å \leq z \leq 16Å$). Partitioning free-energy profiles of $O_2$ calculated from ELS simulations and ILS indicate that more $O_2$ molecules reside in the membrane (shaded orange) than in the aqueous phase (shaded blue). **b)** A representative ELS simulation system in the presence of cytochrome $ba_3$. All systems with different initial ratio of $O_2$ show that $O_2$ is more distributed in the membrane than in the aqueous phase.

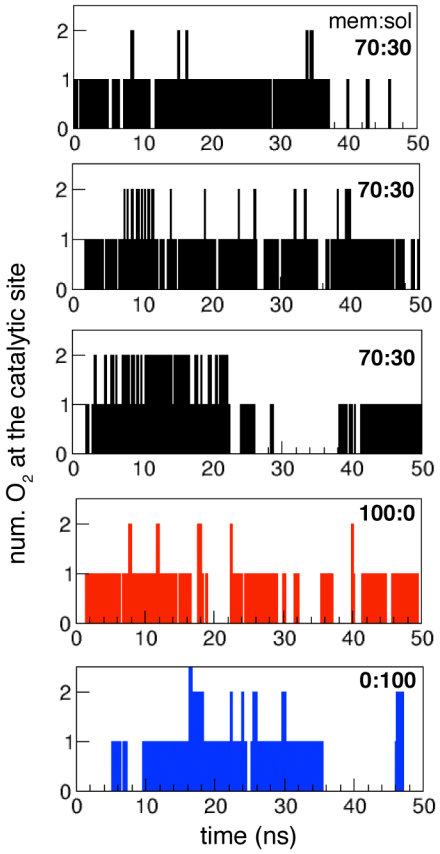


**Figure 2. Entry of $O_2$ into the active site observed during the ELS simulations**

Three of the five simulations are with 70 $O_2$ molecules initially in the membrane and 30 in the aqueous phase, one is with all 100 $O_2$ molecules initially in the membrane, and one with all 100 $O_2$ molecules initially in the aqueous phase. $O_2$ is considered to be the active site when it is within 6Å of $Cu_B$.

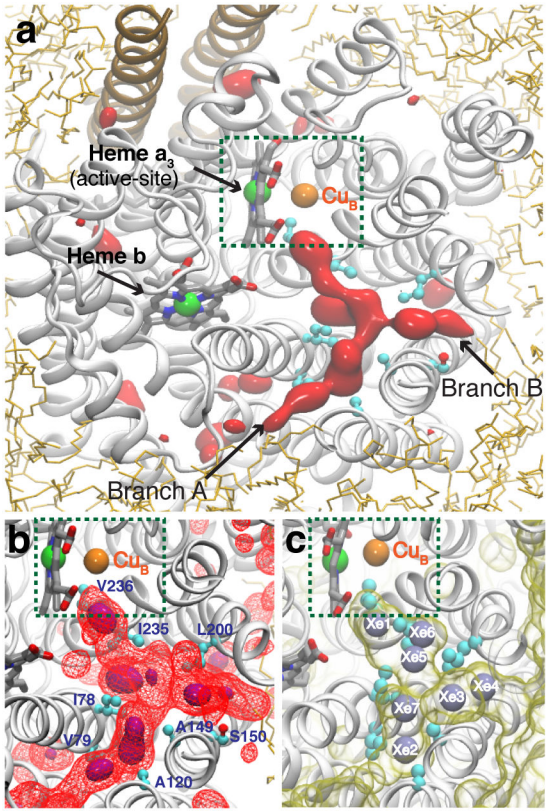


**Figure 3. $O_2$ delivery pathway of cytochrome $ba_3$ identified by the ELS simulations**

All images were taken from the same top view of the enzyme. **a)** Highly occupied $O_2$ regions characterized by the 3D density map calculated using the combined last 40-ns trajectories of five independent simulations. One region, which appears in a Y-shaped form, is the pathway that has been found to deliver $O_2$ to the active site (green-dashed box). It is connected to the membrane via two branches, which we refer to and label as Branches A and B. Red-solid isosurfaces represent $O_2$ partitioning free energy ($\Delta G_{i,sol}$) of −3.5 kcal/mol. **b)** The $O_2$ delivery pathway. Purple-solid and red-wireframe isosurfaces correspond to $\Delta G_{i,sol}$ of −4.0 and −3.0 kcal/mol, respectively. **c)** Xe binding sites identified by X-ray crystallography.[35,40] Xe atoms were detected in a hydrophobic tunnel, displayed as a yellow-transparent surface using a probe radius of 1.8Å; they are numbered according to PDB entry 3BVD.[35] The $O_2$ delivery pathway identified in the present study (b) largely overlaps with this Xe-bound tunnel.

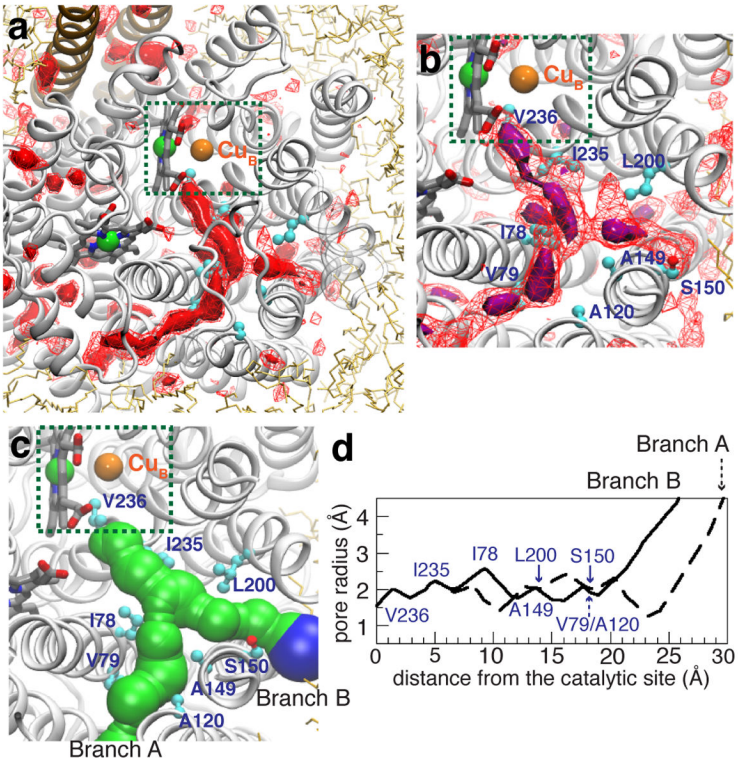


**Figure 4. Favorable $O_2$ partitioning regions in cytochrome $ba_3$ characterized by ILS**

**a)** Highly probable $O_2$ binding regions characterized by the 3D free-energy map calculated by ILS. Red-solid and red-wireframe isosurfaces correspond to $\Delta G_{i,sol}$ of −3.5 and −3.0 kcal/mol, respectively. **b)** Region in the 3D free-energy map that is equivalent to the $O_2$ delivery pathway characterized by ELS: purple-solid and red-wireframe isosurfaces correspond to $\Delta G_{i,sol}$ of −4.0 and −3.0 kcal/mol, respectively. **c)** $O_2$ delivery pathway calculated by MolAxis[60] for the crystal structure and displayed as corridors. Green corridors represent pore radii of 1.2–3.0Å. Blue corridors represent pore radii of >3.0Å. **d)** Pore profiles of Branches A and B of the $O_2$ delivery pathway.

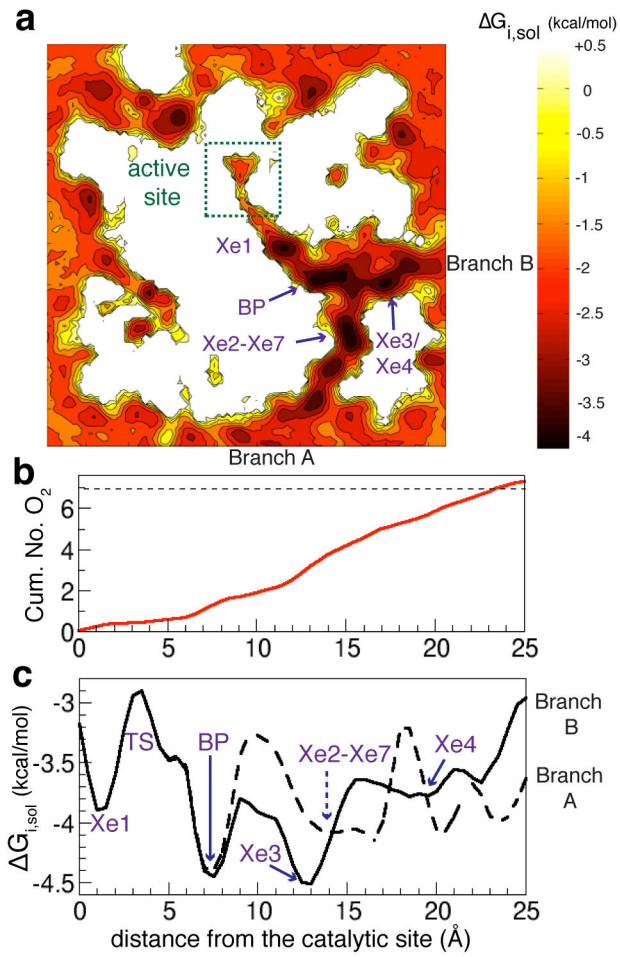


**Figure 5. Energetic profiles of $O_2$ along the delivery pathway**

**a)** A 2D projection of the free-energy map, calculated using MATLAB, describing the partitioning of $O_2$ in the enzyme and its surroundings. The map was calculated by collapsing the normalized 3D density profiles of $O_2$ calculated from ELS over a 50×50×30Å$^3$ grid, which spans the enzyme region covering the entire $O_2$ delivery pathway, heme cofactors, $Cu_B$, and surrounding lipids. Dark colors indicate high probability $O_2$ regions. Light colors indicate $O_2$ scarce regions. **b)** Estimated number of $O_2$ binding sites along the pathway calculated by integrating $O_2$ probability densities ($p_d$) from the active site to the entrances of the pathway. **c)** 1D free-energy profiles of $O_2$ partitioning along its delivery pathway. The coordinates of $O_2$ that have been within 3Å of pathway's residues are clustered into normalized $O_2$ density profiles with respect to the aqueous phase using the distance from the active site (d) as the reaction coordinate. $d=(((x-x_0)^2+(y-y_0)^2+(z-z_0)^2)^{1/2})-6$. ($x_0$, $y_0$, $z_0$) is the position of $Cu_B$ cofactor. $O_2$ is considered to be in the active site when it has been within 6Å of $Cu_B$. BP specifies intersection point of Branches A and B, referring to as "branch-point". $\Delta\Delta G^{TS-BP}$ = +1.5 kcal/mol. The average speed of $O_2$ diffusion along the pathway ($v_0$) is 0.39 (0.29)Å/ps.

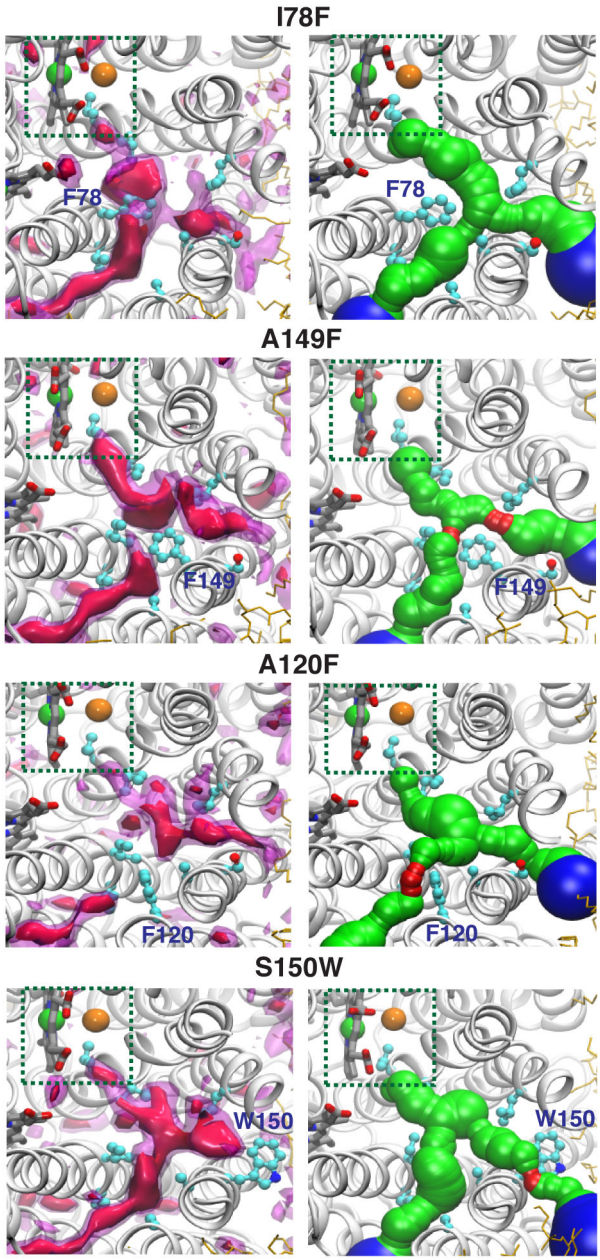


**Figure 6. Alterations of the $O_2$ delivery pathway by *in silico* mutagenesis of pathway-lining residues to bulky substitutions**

Left panels highlight predicted $O_2$ binding regions calculated by ILS performed on the 10-ns of apo trajectories. The pink transparent surface indicates regions with $\Delta G_{i,sol}$ of −2.5 kcal/mol for $O_2$ binding. Right panels show the $O_2$ delivery pathway calculated from the equilibrated structure (at t = 10 ns) of each mutant using MolAxis.[60] Red corridors represent pore radii of <1.2Å. Green corridors represent pore radii of 1.2–3.0Å. Blue corridors represent pore radii of >3. 0Å.

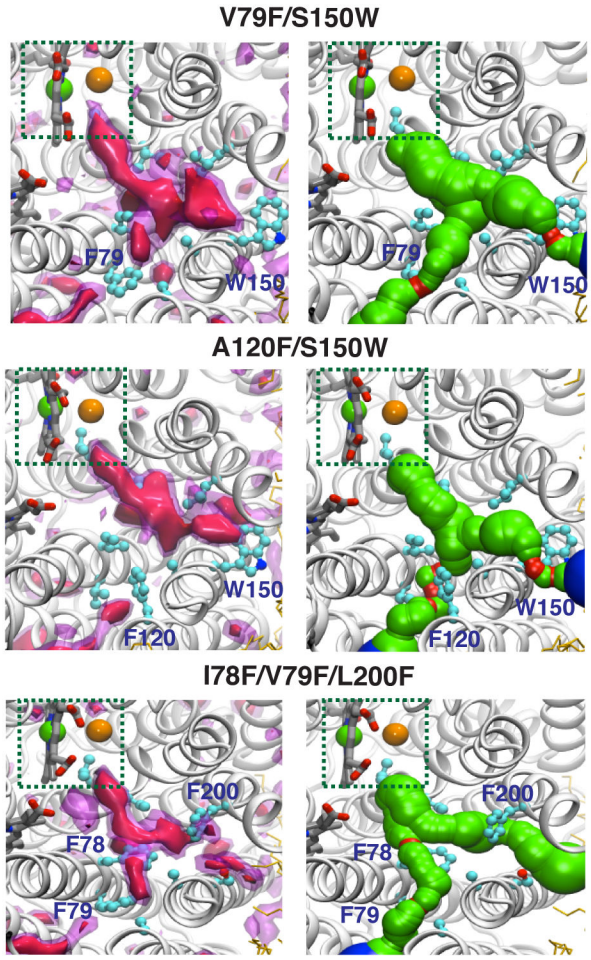


**Figure 7. Alterations of the $O_2$ delivery pathway upon *in silico* blockages of pathway's entrances**

Double (V79F/S150W and A120F/S150W) and triple (I78F/V79F/L200F) mutants have been introduced to hinder the $O_2$ delivery pathway. Descriptions of left and right panels are the same as in Fig 6.

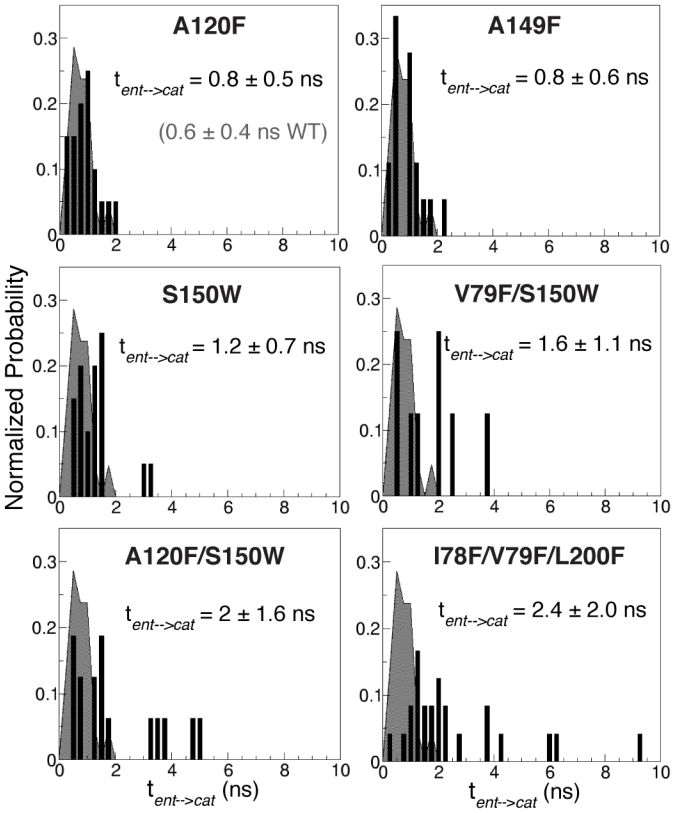


**Figure 8. Migration profiles of $O_2$ along the delivery pathway in the wild-type and mutants of cytochrome $ba_3$ explicitly determined from multiple short ELS simulations**

$t_{ent \rightarrow cat}$ is the transit time of $O_2$ from the entrances of the pathway to the active site. It is directly measured from the first delivered $O_2$ molecule in each simulation. Histograms in each plot represent $t_{ent \rightarrow cat}$ distribution of a mutant. The shaded curved behind the bar histogram represents $t_{ent \rightarrow cat}$ distribution of the wild-type enzyme, providing a direct comparison with each mutant. $t_{ent \rightarrow cat}$ for the wild-type is 0.6±0.4 ns.

**Table 1**

$O_2$ delivery events observed during the long ELS simulations

| System | Delivery events | Unique delivery $O_2$ |
|---|---|---|
| 1) 70:30 | 29 | 26 |
| 2) 70:30 | 34 | 27 |
| 3) 70:30 | 28 | 23 |
| 4) 100:0 | 36 | 28 |
| 5) 0:100 | 21 | 18 |
| **sum** | **122** | **148** |
| **average** | **24.4** | **29.6** |

Systems=initial $O_2$ mem:sol ratio. Unique delivered $O_2$ = number of distinguishable $O_2$ molecules (different ID numbers) found in the active site. Delivery events=number of $O_2$ delivery events observed during the 50-ns simulations. A few $O_2$ molecules made multiple entries to both the enzyme and active site.

**Table 2**

$O_2$ migration times estimated from the ensemble of 21 short ELS simulations

| Branch | Sim. | $t_{first}$ (ns) | $t_{ent \rightarrow cat}$ | $t_{BP \rightarrow cat}$ | $t_{ent \rightarrow BP}$ |
|---|---|---|---|---|---|
| A | 7 | 2.1±0.9 | 0.7±0.2 | 0.4±0.2 | 0.3±0.3 |
| B | 14 | 1.5±0.7 | 0.6±0.2 | 0.4±0.3 | 0.2±0.2 |
| **total** | **21** | **1.7±0.8** | **0.6±0.4** | **0.4±0.3** | **0.2±0.2** |

These results are determined from the first delivered $O_2$ molecules in all the simulations. Sim.=number of simulations. $t_{first}$ =time taken to observe the first $O_2$ reaching the active site after the start of a simulation. $t_{ent \rightarrow cat}$ =transit time of $O_2$ diffusion from the entrance to the active site. $t_{BP \rightarrow cat}$ =transit time of $O_2$ diffusion to the BP to the active site. $t_{ent \rightarrow BP}$ =transit time of $O_2$ from the entrances to the intersection point of Branches A and B.

**Table 3**

Alterations of $O_2$ access by *in silico* mutagenesis

| Mutant | Sim | $t_{first}$ | Branch | $t_{ent \rightarrow cat}$ | $t_{BP \rightarrow cat}$ | $t_{ent \rightarrow BP}$ |
|---|---|---|---|---|---|---|
| A120F | 20 | 3.2±2.0 | B | 0.8±0.5 | 0.5±0.3 | 0.3±0.2 |
| A149F | 20 | 2.6±2.0 | A/B | 0.8±0.6 | 0.3±0.4 | 0.5±0.4 |
| S150W | 20 | 2.7±1.1 | A | 1.2±0.7 | 0.8±0.8 | 0.4±0.3 |
| A120F/S150W | 18 | 3.8±2.0 | B | 2.0±1.6 | 1.0±1.0 | 1.0±1.1 |
| V79F/S150W | 8 | 4.0±2.3 | (A)/B | 1.6±1.1 | 0.4±0.2 | 1.2±1.0 |
| I78F/V79F/L200F | 29 | 6.7±3.9 | (A)/B | 2.4±2.0 | 0.6±0.8 | 1.8±2.0 |

The results are from the short ELS simulations. Sim=number of independent simulations. Branch(es)= entrance(s) of the first observed $O_2$ molecule entering the active site in each simulation. In the A120F/S150W mutant, O2 delivery was observed in only 8 of its 10-ns simulations. In the V79F/S150 mutant, O2 delivery was observed in only 18 of its 20-ns simulations. In the triple mutant, $O_2$ delivery was observed in 29 of its 15-ns simulations. Of all repeated simulations, $O_2$ entry via Branch A was found only in one simulation for V79F/S150W and triple mutants.

*Biochemistry*. Author manuscript; available in PMC 2016 December 07.